Pergamon

*Int. J. Solids Structures* Vol. 34, No. 12, pp. 1419–1440, 1997

0020–7683/97 $17.00 + .00

PII: S0020–7683(96)00094–7

# THE BRAZIER EFFECT FOR FINITE LENGTH COMPOSITE CYLINDERS UNDER BENDING

B. F. TATTING and Z. GÜRDAL
Department of Engineering Science and Mechanics, Virginia Polytechnic Institute and State University, Blacksburg, VA 24060-0219, U.S.A.

and

V. V. VASILIEV
Department of Aerospace Composite Structures, Moscow State University of Aviation Technology, Moscow, Russia 103767

(*Received* 25 *October* 1995; *in revised form* 3 *May* 1996)

**Abstract**—The derivation for the nonlinear bending response of finite length composite tubes exhibiting cross-sectional deformations associated with Brazier's flattening effect is presented using classical shell theory. Semi-membrane constitutive theory is used to simplify the analysis and local buckling on the compressive side of the tube is investigated based on the axial stress and local curvature on the compressive side of the cylinder. The nonlinear system is solved numerically and results are obtained for various combinations of material and geometric parameters as well as end conditions. Results of the present investigation are compared with published finite element solutions and approximate analytical solutions for the Brazier effect of finite length tubes. © 1997 Elsevier Science Ltd. All rights reserved.

## 1. INTRODUCTION

The Brazier effect is a nonlinear phenomenon associated with the bending of long tubes with deformable cross-sections. It differs from usual nonlinear shell problems in that the nonlinear response is induced by the macroscopic rotation of the structure, as opposed to classical boundary layer effects due to the local rotations of shell elements near the boundaries. To illustrate, shown in Fig. 1 is an infinitesimal section of a deformed circular cylinder along with the linear stress state associated with pure bending. Due to the curvature of the tube axis, the compressive and tensile stresses act at an angle to the unrotated cross-section and deform the original circular shape into an oval. This ovalization, in turn, decreases the moment of inertia of the cross-section and leads to a nonlinear load-displacement relation. Additionally, the deformation of the cross-section increases the axial bending stresses and lowers the structure's buckling load. Thus, reliable design of long thin-walled composite tubes must include consideration of the Brazier effect on all aspects of possible failure modes.

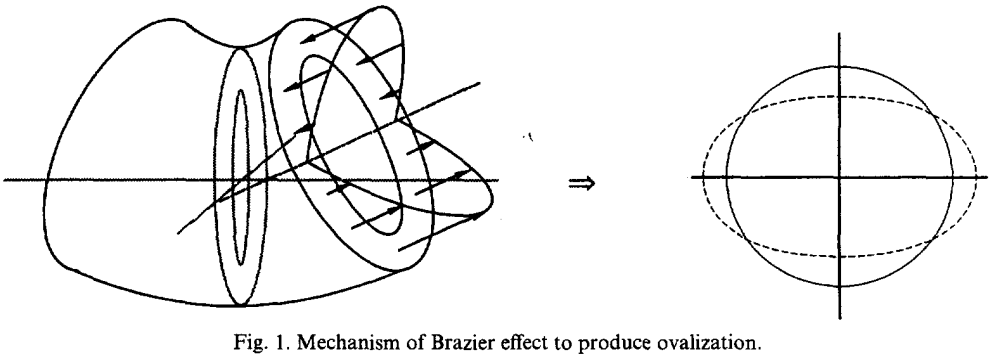

Fig. 1. Mechanism of Brazier effect to produce ovalization.

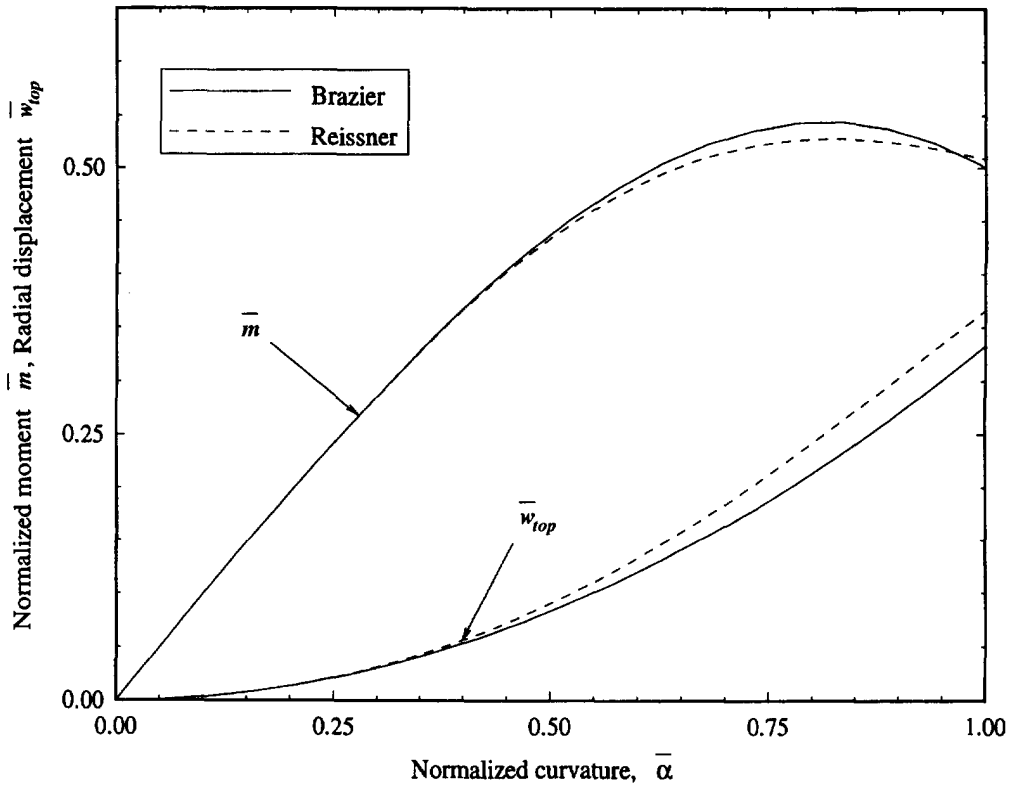


Fig. 2. Moment and radial displacement vs curvature for long isotropic cylinder.

The approach used in the present paper involves the solution of this highly nonlinear problem using the simplifications proposed by L. G. Brazier (1926) for finitely long shells. It has been unequivocally shown (see the excellent discussion by Calladine, 1983) that Brazier's somewhat crude approximations lead to simple equations that agree remarkably well with the robust nonlinear solution first formulated by Reissner (1959). Fabian's (1977) numerical solution of Reissner's equation is compared to Brazier's solution for the moment and cross-sectional deformation vs end rotation in Fig. 2. The radial displacement is a measure of the ovalization of the cross-section and one can see that Brazier's approximation underestimates the deformation by around 12% at the limit point, while overestimating the moment by approximately 3%. However, the gains in analytical simplicity and computational efficiency for the approximate solution are well worth the small errors. Throughout this paper we refer to Brazier's approximations to justify neglecting certain terms, such as powers or derivatives of certain functions. It can be shown that retaining these higher-order terms will result in significant disagreement between Brazier's solution and the accurate nonlinear solution of Reissner. For example, Bannister (1984) used a variational approach analogous to Brazier's formulation (actually based on the work of Wood (1958), who included the effects of internal pressure), including all the quadratic terms that are neglected here. The resulting moment-curvature relations underestimate the nonlinearity considerably and predict a limit moment with over 30% error. Further discussion of the differences between these two solutions for infinite length tubes can be found in a recent paper by the authors (Tatting *et al.*, 1996).

The application of the Brazier effect of finite length tubes was first investigated by Aksel'rad (1965), who employed Vlasov's semi-membrane constitutive theory to determine the effect of the cross-sectional deformation on the structure's buckling load. Other notable researchers (Aksel'rad & Emmerling, 1984; Libai & Bert 1994) have also employed semi-membrane theory to simplify the analysis and we will do the same for this investigation. Semi-membrane (or semi-momentless) theory is a simplified constitutive law that neglects bending stiffness of the shell wall in the axial direction, thereby eliminating the boundary

layer present in usual shell problems. It reduces the order of the equations in the axial direction from eight to four and allows only the membrane boundary conditions to be stipulated at the ends. Semi-membrane theory also assumes that the circumferential strain is negligible and as a result, the Poisson effect is often ignored. Its application is for long shells or ones in which the variation of the stresses and strains is slow in the axial direction (for further details, see Vasiliev, 1993).

The goal of this paper is to determine the effect of material and geometric parameters on the bending response and buckling loads of finite length orthotropic cylinders. The governing equations include the Brazier effect and are derived from classical nonlinear shell theory (as opposed to direct variational methods that are commonly used for this problem) and we include the possibility of shear warping of the cross-section, as introduced by Libai and Bert (1994). Efficient numerical techniques are used to solve the resulting pair of coupled ordinary differential equations, and the results for the governing parameters are presented for various boundary conditions and material systems.

## 2. NONLINEAR SHELL THEORY SOLUTION

We begin with the derivation of the governing equations through classical shell equations along with the semi-membrane constitutive assumptions. The governing equations are expressed in terms of the cylindrical displacements $(u, v, w)$, which will be expanded in a trigonometric series in the circumferential direction. We also utilize Brazier's simplifications by ignoring products of higher-order terms and by assuming inextensional deformation of the cross-section.

### 2.1. *Strain-displacement relations*

The geometry of the shell is displayed in Fig. 3, where the deformation is symmetric about $x = L/2$. The dotted line represents the beam-type deflection of the neutral surface in the $Z$-direction, which is defined here as $-v(x, \theta = \pi/2)$. We can then define the beam rotation and curvature in terms of the $v$ displacement:

$$\Omega(x) = \left.\frac{\partial v}{\partial x}\right|_{\theta=\pi/2} \qquad \kappa(x) = \frac{-\mathrm{d}\Omega}{\mathrm{d}x} = -\left.\frac{\partial^2 v}{\partial x^2}\right|_{\theta=\pi/2}. \tag{1}$$

The end rotations can be expressed through the application of the symmetry condition

$$\bar{\Omega} = \frac{\Omega(0) - \Omega(L)}{2} = -\frac{1}{2}\int_0^L \left(\frac{\mathrm{d}\Omega}{\mathrm{d}x}\right)\mathrm{d}x = \int_0^{L/2} \kappa(x)\,\mathrm{d}x. \tag{2}$$

Also note that the compressive stress state is located at the top of the structure which corresponds to $\theta = 0$.

We now specialize the kinematic relations with respect to the Brazier-type deformation that we expect. Sander's (1963) nonlinear strain-displacement relations for thin shells with

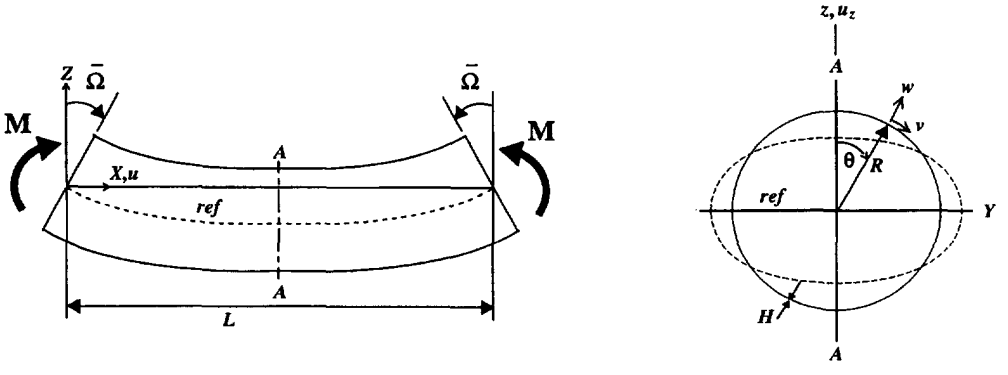


Fig. 3. Geometry of deformed shell.

small strains and moderate rotations are used. The surface strain quantities can be expressed through the cylindrical displacements as

$$\varepsilon_x = \frac{\partial u}{\partial x} + \frac{1}{2}\left(\frac{\partial w}{\partial x}\right)^2, \qquad \kappa_x = -\frac{\partial^2 w}{\partial x^2},$$

$$\varepsilon_\theta = \frac{1}{R}\left(\frac{\partial v}{\partial \theta} + w\right) + \frac{1}{2R^2}\left(v - \frac{\partial w}{\partial \theta}\right)^2, \quad \kappa_\theta = -\frac{1}{R^2}\left(\frac{\partial^2 w}{\partial \theta^2} - \frac{\partial v}{\partial \theta}\right),$$

$$\gamma_{x\theta} = \frac{1}{R}\frac{\partial u}{\partial \theta} + \frac{\partial v}{\partial x} - \frac{1}{R}\left(v - \frac{\partial w}{\partial \theta}\right)\frac{\partial w}{\partial x}, \quad \kappa_{x\theta} = -\frac{1}{R}\left(2\frac{\partial^2 w}{\partial \theta \partial x} - \frac{\partial v}{\partial x}\right). \tag{3}$$

The nonlinear terms in the surface strains correspond to axial and circumferential rotations of a shell element. To conform to Brazier's level of approximation, the only nonlinear term that we need to keep is for the shear strain. Thus the strains and curvatures become

$$\varepsilon_x = \frac{\partial u}{\partial x}, \quad \varepsilon_\theta = \frac{1}{R}\left(\frac{\partial v}{\partial \theta} + w\right), \quad \gamma_{x\theta} = \frac{1}{R}\frac{\partial u}{\partial \theta} + \frac{\partial v}{\partial x} - \frac{1}{R}\left(v - \frac{\partial w}{\partial \theta}\right)\frac{\partial w}{\partial x},$$

$$\kappa_x = -\frac{\partial^2 w}{\partial x^2}, \quad \kappa_\theta = -\frac{1}{R^2}\left(\frac{\partial^2 w}{\partial \theta^2} - \frac{\partial v}{\partial \theta}\right), \quad \kappa_{x\theta} = -\frac{1}{R}\left(2\frac{\partial^2 w}{\partial \theta \partial x} - \frac{\partial v}{\partial x}\right). \tag{4}$$

We now expand the displacements in terms of a Fourier series in the circumferential direction. We truncate the trigonometric series after only two terms for $v$ and $w$, however for $u$ the third term is needed as a consequence of the definition for the shear strain in eqn (4) (which will become evident shortly).

$$\begin{aligned} u(x,\theta) &= u_1(x)\cos\theta + u_2(x)\cos 2\theta + u_3(x)\cos 3\theta \\ v(x,\theta) &= v_1(x)\sin\theta + v_2(x)\sin 2\theta \\ w(x,\theta) &= w_1(x)\cos\theta - w_2(x)\cos 2\theta. \end{aligned} \tag{5}$$

The work of Aksel'rad (1965) has shown that additional terms in the series for $v$ and $w$ are required only for shorter cylinders. However, these short cylinders experience a substantial bending boundary layer due to the edge effects, where the semi-membrane solution may not be valid. Therefore, the two-term expansion will be considered adequate, while keeping in mind that the analysis may not be accurate for short cylinders.

We now invoke Brazier's condition of inextensionality of the cross-section. This implies that the circumferential strain is zero, so that

$$\varepsilon_\theta = \frac{1}{R}[(v_1 + w_1)\cos\theta + (2v_2 - w_2)\cos 2\theta] = 0. \tag{6}$$

Therefore, the inextensionality condition generates two algebraic relations for the unknown displacements.

$$v_1 = -w_1, \quad v_2 = w_2/2. \tag{7}$$

Here we will eliminate $v_1$ and $v_2$ and formulate the strain measures of eqn (4) in terms of the radial displacement components $w_1$ and $w_2$. We do this since radial displacement gives a greater physical feel to the problem than circumferential displacement. However it should be noted that the resulting equations will be membrane equations, and that the boundary conditions (in terms of $w_i$) are physically related to the circumferential displacements $v_i$.

Applying eqns (5) and (7) to eqn (4) and ignoring products of higher order terms (akin to Brazier) results in Fourier representations of the non-zero strain quantities:

$$\varepsilon_x = \frac{du_1}{dx}\cos\theta + \frac{du_2}{dx}\cos 2\theta + \frac{du_3}{dx}\cos 3\theta$$

$$\gamma_{x\theta} = \left[-\frac{u_1}{R} - \frac{dw_1}{dx}\left(1 - \frac{3w_2}{4R}\right)\right]\sin\theta + \left[-\frac{2u_2}{R} + \frac{1}{2}\frac{dw_2}{2dx}\right]\sin 2\theta + \left[-\frac{3u_3}{R} + \frac{dw_1}{dx}\frac{3w_2}{4R}\right]\sin 3\theta$$

$$\kappa_x = -\frac{\partial^2 w_1}{\partial x^2}\cos\theta + \frac{\partial^2 w_2}{\partial x^2}\cos 2\theta,$$

$$\kappa_\theta = -\frac{3w_2}{R^2}\cos 2\theta, \quad \kappa_{x\theta} = \frac{1}{R}\left(\frac{dw_1}{dx}\sin\theta - \frac{7}{2}\frac{dw_2}{dx}\sin 2\theta\right). \tag{8}$$

Note that the nonlinear shear strain contains variations for the harmonic $\sin 3\theta$, so that the third term for the expansion of $u$ must be included. Thus the mid-surface strain quantities are all in terms of five unknown functions of $x$.

2.2. *Constitutive relations*

The stress–strain behavior for these shells is based on classical lamination theory along with the semi-membrane assumptions mentioned earlier. Macroscopic laminate stiffness measures are determined by integrating through the thickness of the shell wall in the usual manner. In particular, we calculate the extensional and bending stiffnesses as

$$A_{ij} = \int_{-H/2}^{H/2} \bar{Q}_{ij}\,dr \quad D_{ij} = \int_{-H/2}^{H/2} \bar{Q}_{ij} r^2\,dr \tag{9}$$

where $\bar{Q}_{ij}$ are the transformed reduced stiffnesses of an orthotropic layer (see Jones, 1975) and the $r$-direction is through the thickness of the laminate. We further restrict our investigation to balanced symmetric laminates. The relation of the in-plane stress resultants to the surface strain measures is then

$$\begin{bmatrix} N_x \\ N_\theta \\ N_{x\theta} \end{bmatrix} = \begin{bmatrix} A_{11} & A_{12} & 0 \\ A_{12} & A_{22} & 0 \\ 0 & 0 & A_{66} \end{bmatrix} \begin{bmatrix} \varepsilon_x \\ \varepsilon_\theta \\ \gamma_{x\theta} \end{bmatrix}, \quad \begin{bmatrix} M_x \\ M_\theta \\ M_{x\theta} \end{bmatrix} = \begin{bmatrix} D_{11} & D_{12} & D_{16} \\ D_{12} & D_{22} & D_{26} \\ D_{16} & D_{26} & D_{66} \end{bmatrix} \begin{bmatrix} \kappa_x \\ \kappa_\theta \\ \kappa_{x\theta} \end{bmatrix}. \tag{10}$$

We now invoke the assumptions of semi-membrane constitutive theory. First, shell bending and twisting in the axial direction are ignored. This can be expressed mathematically as

$$D_{11}, D_{12}, D_{16}, D_{26}, D_{66} \to 0. \tag{11}$$

Thus, the bending and twisting moments in the axial direction ($M_x, M_{xy}$) are zero. Also, since the assumptions of semi-membrane theory suppress the Poisson effect, the in-plane stress resultants depend only on their corresponding strain measures:

$$N_x = E_x H\varepsilon_x \quad N_\theta = E_\theta H\varepsilon_\theta \quad N_{x\theta} = G_{x\theta} H\gamma_{x\theta}. \tag{12}$$

Here we define the effective moduli in terms of the extensional stiffness measures to include arbitrary laminate layups:

$$E_x = \frac{A_{11}A_{22} - A_{12}^2}{A_{22}H} \quad E_\theta = \frac{A_{11}A_{12} - A_{12}^2}{A_{11}H} \quad G_{x\theta} = \frac{A_{66}}{H}. \tag{13}$$

The inextensionality condition in the circumferential direction is satisfied at the constitutive level by the assumption that $E_\theta \to \infty$. Standard semi-membrane theory also assumes zero shear strain (i.e. $G_{x\theta} \to \infty$), though for this problem that assumption is invalid. The importance of shear strain was first surmised by Libai and Bert (1994) for arbitrary beam loading, but the inclusion is also needed under pure bending. For instance, a vertical shear force applied to the structure would produce shear stresses and strains varying quadratically across the cross-section to produce warping, much like classical beam analysis (see Fig. 4a). This deformation corresponds to the $\sin\theta$ term of the shear strain in eqn (8). For beams under pure bending (in which the shear force is identically zero), this type of shear deformation does not exist and the assumption of zero shear strain should be valid (this will be seen to be true for the $\sin\theta$ term of eqn (8)). However due to the Brazier effect a different mode of shear warping exists, in which the shear stresses vary as $\sin 2\theta$ (see Fig. 4b). This is a consequence of the presence of the end restraints which maintain the circular shape of the cross-section. The transformation of the cross-section from an oval in the middle of the cylinder into a circle at the ends induces these localized shear stresses. As we shall see, neglecting this shear deformation results in erroneous results of finite length tubes under bending.

Therefore, including the shear strain completes the necessary constitutive relations for an orthotropic shell:

$$N_x = E_x H\varepsilon_x \quad N_{x\theta} = G_{x\theta} H\gamma_{x\theta} \quad M_\theta = D_{22}\kappa_\theta. \tag{14}$$

2.3. *Equilibrium equations*

The nonlinear equilibrium equations for thin shells under semi-membrane constitutive theory are presented by Vasiliev (1993) as

$$\begin{aligned}
\frac{\partial}{\partial\theta}(A_1 N_\theta) + \frac{\partial}{\partial x}(A_2 N_{x\theta}) - \frac{\partial A_1}{\partial\theta} N_x + \frac{A_1 A_2}{R_\theta} Q_\theta &= 0 \\
\frac{\partial}{\partial x}(A_2 N_x) + \frac{\partial}{\partial\theta}(A_1 N_{x\theta}) + \frac{\partial A_1}{\partial\theta} N_{x\theta} &= 0 \\
\frac{\partial}{\partial\theta}(A_1 M_\theta) - A_1 A_2 Q_\theta &= 0 \\
\frac{\partial}{\partial\theta}(A_1 Q_\theta) - A_1 A_2\left(\frac{N_\theta}{R_\theta} + \frac{N_x}{R_x}\right) + A_1 A_2 p &= 0
\end{aligned} \tag{15}$$

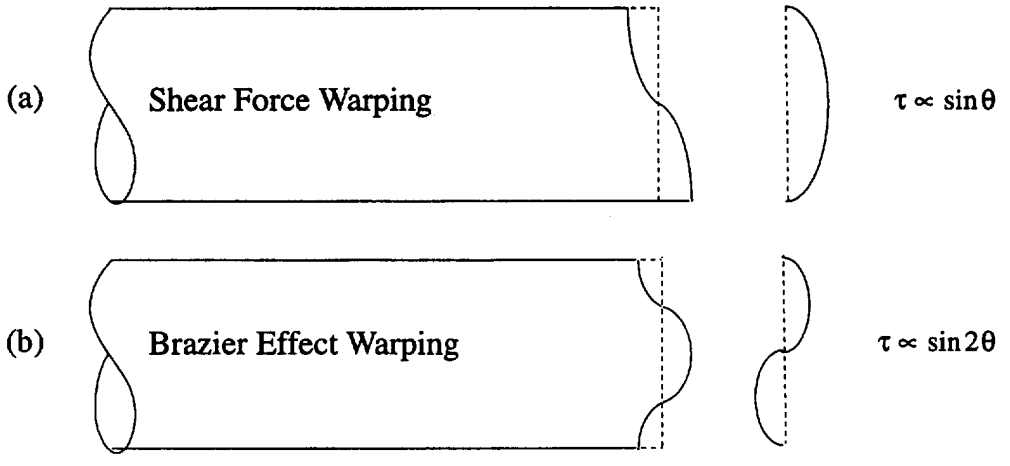


Fig. 4. Cross-sectional warping under bending.

where the bending and twisting terms in the axial direction have been removed. Here $A_1$ and $A_2$, $R_x$ and $R_\theta$ are the Lamé coefficients and Gaussian curvatures of the surface defined by the shell in $(x, \theta)$ coordinates. In the standard nonlinear formulation for cylindrical shells, these surface parameters are calculated as

$$A_1 = 1 \quad \frac{1}{R_x} = \kappa_x \quad A_2 = R \quad \frac{1}{R_\theta} = \frac{1}{R} + \kappa_\theta. \tag{16}$$

However, the driving mechanism for the Brazier effect relies on the action of the axial stresses along with the curvature of the axis and shape of the cross-section. Thus the surface parameters must be derived by assuming a circular shell with some axial curvature and cross-sectional deformation. Referring to the geometry of Fig. 3, we assume that the cross-section rotates through an angle equal to the slope of the reference line, $\Omega(x)$. We also assume that the cross-section deforms, so that the distance from the reference line is

$$z = R\cos\theta + u_z = (R+w)\cos\theta - v\sin\theta. \tag{17}$$

(As will be shown, there is additional deformation in the form of warping of the cross-section near the ends of the cylinder, however it can be shown that these terms can be ignored in the calculation of $A_1$.) Then, the definition for the deformed shell becomes:

$$\begin{aligned} X &= x - \sin\Omega[(R+w)\cos\theta - v\sin\theta] \\ Y &= (R+w)\sin\theta + v\cos\theta \\ Z &= -v_1(x) + \cos\Omega[(R+w)\cos\theta - v\sin\theta]. \end{aligned} \tag{18}$$

Calculation of the Lamé coefficients and Gaussian curvatures in the usual manner (see Novoshilov, 1959), along with the assumption of small rotations, gives a different expression for $A_1$:

$$A_1 = 1 - \kappa R\left[\frac{w_1}{R} + \left(1 - \frac{3w_2}{4R}\right)\cos\theta - \frac{w_2}{4R}\cos 3\theta\right]. \tag{19}$$

Note that this differs from the usual Lamé parameter for circular cylindrical shells since $\partial A_1/\partial\theta \neq 0$ here.

The four equilibrium equations, eqn (15), are combined into two nonlinear equations by eliminating the intermediate variables $N_\theta$ and $Q_\theta$. Some terms are also neglected due to their relative size. For instance, the equilibrium equations contain many terms which are multiplied by $A_1$. However, since $\kappa R$ is much smaller than unity, we can neglect the second part of $A_1$ for most terms. The exception is when $A_1$ has circumferential derivatives which are multiplied by $N_x$. This derivative of $A_1$ is not equal to zero (though it is for standard cylindrical shell equations) and the multiplication of it with the largest stress measure generates a term which cannot be neglected. Therefore, following this argument, the equilibrium equation in the axial direction is

$$\frac{\mathrm{d}}{\mathrm{d}x}(N_x) + \frac{1}{R}\frac{\partial}{\partial\theta}(N_{x\theta}) = 0. \tag{20}$$

The intermediate stress variables are eliminated through the use of the third and fourth equilibrium equations, which become

$$Q_\theta = \frac{1}{R}\frac{\partial M_\theta}{\partial \theta} \quad N_\theta = \frac{R_\theta}{R^2}\frac{\partial^2 M_\theta}{\partial \theta^2} + pR_\theta - \frac{R_\theta}{R_x}N_x. \tag{21}$$

Insertion of these stress measures into the first of eqn (15) yields an equation for equilibrium in the circumferential direction:

$$\frac{1}{R}\frac{\partial}{\partial \theta}\left(\frac{R_\theta}{R^2}\frac{\partial^2 M_\theta}{\partial \theta^2}\right) + \frac{1}{R^2}\frac{\partial M_\theta}{\partial \theta} + \frac{1}{R}\frac{\partial}{\partial \theta}(pR_\theta) + \frac{\partial}{\partial x}(N_{x\theta}) = \frac{1}{R}\frac{\partial A_1}{R\partial \theta}N_x + \frac{1}{R}\frac{\partial}{\partial \theta}\left(\frac{R_\theta}{R_x}N_x\right). \tag{22}$$

Substitution of the constitutive laws eqn (14) and the definitions of the mid-surface strains eqn (8) into the two equilibrium equations yields the necessary equations for the solution of the unknown displacements.

2.4. *Boundary conditions*

The Fourier series expansion of the displacements demands that the boundary and symmetry conditions also be expressed in this manner. In the circumferential direction, the conditions of periodicity have automatically been fulfilled by the series representation in terms of sine and cosine. In the axial direction, edge conditions are required at the end of the tube ($x = 0$) and at the line of symmetry ($x = L/2$). These conditions are deduced from Fig. 3 as

$$\begin{aligned} &u(0,\theta) = \bar{\Omega}R\cos\theta \\ &\qquad\text{-or-} \\ &N_x(0,\theta) = \frac{-M}{\pi R^2}\cos\theta \end{aligned} \qquad v(0,\theta) = 0; \quad u(L/2,\theta) = 0; \quad \frac{\partial v}{\partial x}(L/2,\theta) = 0. \tag{23}$$

A remark is needed in regard to the boundary conditions at $x = 0$. Often the governing equations are formulated solely in terms of the radial displacement $w(x,\theta)$ by assuming that the shear stress is zero. In such a situation it can be shown that the first two options of eqn (23) need to be replaced with $\partial w/\partial x = 0$ or $\partial^2 w/\partial x^2 = 0$, which are often construed as clamped or simply supported boundary conditions. Since semi-membrane theory cannot account for bending of the shell wall in the axial direction, these classifications of "clamped" and "simply-supported" ends are not appropriate terminology for the boundary conditions. The concept of clamped vs simply-supported can only be related to the structure as a beam, that is, through the designations of $\Omega$ and $M$ at the ends (for this case of pure bending, the beam would be considered clamped). Therefore, the boundary conditions at $x = 0$ must correspond to membrane boundary conditions and the first two choices of eqn (23) correspond to a fixed or free end in the axial direction, respectively. The first choice demands that the axial displacement vary linearly across the cross-section and that there is no Brazier effect warping (see Fig. 4). This is a "fixed" or "restrained" end, either from a rigid plate or a sturdy ring stiffener. The second choice (in terms of $N_x$) can be achieved by a "free" end or a flexible stiffener. Here $\cos 2\theta$ warping is allowed (see Fig. 4b), but the axial stress must conform to a linear variation. Of course, these are just the limiting cases: for elastic ring stiffeners with finite stiffnesses any intermediate combination of these two conditions is also a possibility. The second boundary condition of eqn (23), $v(0,\theta) = 0$, corresponds to the cross-sectional shape restraint. This equation guarantees that the cross-section does not experience deformation and remains circular, since the displacements $v$ (and $w$ through eqn (7)) are zero at the ends.

The boundary conditions of eqn (23) are expressed in terms of the Fourier representation of the displacements ($u_i$ and $w_i$) as

*θ conditions*:

$$\begin{matrix} u_1(0) = \bar{\Omega}R \\ \text{-or-} \\ \dfrac{du_1}{dx}(0) = \dfrac{-M}{E_x \pi H R^2} \end{matrix} \qquad w_1(0) = 0 \quad u_1(L/2) = 0 \quad \frac{dw_1}{dx}(L/2) = 0. \tag{24}$$

*2θ conditions*:

$$\begin{matrix} u_2(0) = 0 \\ \text{-or-} \\ \dfrac{du_2}{dx}(0) = 0 \end{matrix} \qquad w_2(0) = 0 \quad u_2(L/2) = 0 \quad \frac{dw_2}{dx}(L/2) = 0. \tag{25}$$

*3θ conditions*:

$$\begin{matrix} u_3(0) = 0 \\ \text{-or-} \\ \dfrac{du_3}{dx}(0) = 0 \end{matrix} \qquad u_3(L/2) = 0. \tag{26}$$

2.5. *Governing equations*

Let us first examine the equilibrium equation in the circumferential direction, eqn (22). Grouping terms as functions of the first three harmonics $(\theta, 2\theta, 3\theta)$ and setting the coefficients to zero yields the following ordinary differential equations:

$$G_{x\theta}H\frac{d}{dx}\left[\frac{-u_1}{R} - \frac{dw_1}{dx}\left(1 - \frac{3w_2}{4R}\right)\right] = 0, \tag{27}$$

$$\left(-\frac{18D_{22}}{R^4} - \frac{6p}{R}\right)w_2 + G_{x\theta}H\frac{d}{dx}\left[\frac{-2u_2}{R} - \frac{1}{2}\frac{dw_2}{2dx}\right] = E_xH\frac{du_1}{dx}\left(\frac{d^2w_1}{dx^2} + \frac{\kappa}{2}\right), \tag{28}$$

$$G_{x\theta}H\frac{d}{dx}\left[\frac{-3u_3}{R} + \frac{dw_3}{dx}\left(\frac{3w_2}{4R}\right)\right] = 0. \tag{29}$$

The same technique for the first two harmonics of eqn (20) generates the final two equations

$$E_xH\frac{d^2u_1}{dx^2} + \frac{G_{x\theta}H}{R}\left[\frac{-u_1}{R} - \frac{dw_1}{dx}\left(1 - \frac{3w_2}{4R}\right)\right] = 0 \tag{30}$$

$$E_xH\frac{d^2u_2}{dx^2} + \frac{2G_{x\theta}H}{R}\left[-\frac{2u_2}{R} - \frac{1}{2}\frac{dw_2}{dx}\right] = 0. \tag{31}$$

Thus we have a complete system of five unknowns, five second-order ordinary differential equations and five sets of boundary conditions. One final equation exists, which relates the applied moment to the displacement response of the cylinder:

$$\mathrm{M} = -\oint N_x(R\cos\theta + u_z)R\,d\theta. \tag{32}$$

Note that the moment arm for the axial stress resultant corresponds to the deformed state, which reflects the change in the moment of inertia of the cross-section. After the expansion of the displacements the relation becomes:

$$M = -E_x \pi H R^2 \left[ \frac{du_1}{dx}\left(1 - \frac{3w_2}{4R}\right) - \frac{du_3}{dx}\left(\frac{w_2}{4R}\right) \right]. \tag{33}$$

This is the one-dimensional beam equation. It should be noted that the loading quantity M can, in general, be any function of $x$. A more general approach, using variational methods and including shear forces on the tube, has been developed by Libai and Bert (1994), who also take into account the change of the cross-section on the resistance to the shear loading. Here we restrict our study to pure bending (M = constant).

2.6. *Solution for $\theta$ and $3\theta$ variation*

The equilibrium equations can now be solved analytically for the variables $u_1$, $w_1$ and $u_3$ in terms of the unknown displacements $u_2$ and $w_2$. We begin by integrating eqns (27) and (29) and applying the symmetry conditions of eqns (24) and (26). Thus

$$\frac{u_1}{R} + \frac{dw_1}{dx}\left(1 - \frac{3w_2}{4R}\right) = -\frac{C_1}{G_{x\theta}H} \qquad \frac{3u_3}{R} - \frac{dw_1}{dx}\left(\frac{3w_2}{4R}\right) = -\frac{C_2}{G_{x\theta}H} \tag{34}$$

where $C_1$ and $C_2$ are constants and represent the $\cos\theta$ and $\cos 3\theta$ components of the shear stress. However, application of the boundary conditions at $x = L/2$ determines that both constants are zero (this is not true for beams with shear forces). Thus $u_1$ and $u_3$ are both expressed in terms of $w_1$ and $w_2$. Since $w_1$ can be defined from eqns (7), (5) and (1) as

$$\frac{dw_1}{dx} = -\frac{dv_1}{dx} = -\left.\frac{\partial v}{\partial x}\right|_{\theta=\pi/2} = -\Omega(x) \tag{35}$$

the equations for the axial displacements are

$$u_1 = \Omega(x)R\left(1 - \frac{3w_2}{4R}\right) \qquad \frac{du_1}{dx} \approx -\kappa(x)R\left(1 - \frac{3w_2}{4R}\right)$$

$$u_3 = -\Omega(x)R\left(\frac{w_2}{4R}\right) \qquad \frac{du_3}{dx} \approx \kappa(x)R\left(\frac{w_2}{4R}\right). \tag{36}$$

The derivatives of $w_2$ are neglected to correctly model Brazier's linearization. Similarly, we neglect powers of higher-order terms in eqn (33) so that

$$\frac{M}{E_x \pi H R^3} = \kappa(x)\left(1 - \frac{3w_2}{2R}\right). \tag{37}$$

Note that both the fixed and free end boundary conditions (eqns (24) and (26)) are automatically satisfied by eqn (36), and that the axial equilibrium equation for the $\theta$ variation eqn (30) is not used (instead equilibrium in the axial direction is fulfilled by the beam equation).

2.7. *Solution for $2\theta$ variation*

The combination of the equilibrium equations and boundary conditions, eqns (25), (28) and (31), along with the solutions for $u_1$ and $w_1$ yield the complete system for the solution of the Brazier effect displacements $u_2$ and $w_2$. Let us first introduce some non-dimensional variables which are defined as:

$$\bar{x} = \frac{2x}{L} \quad \bar{u} = \frac{2L}{R^2}u_2 \quad \bar{w} = \frac{w_2}{R}. \tag{38}$$

The end rotation, axial curvature, bending moment and pressure are all normalized with respect to their classical buckling values for an infinite cylinder:

$$\bar{\alpha} = \frac{E_x H R^2 \bar{\Omega}}{L\sqrt{D_{11}E_\theta H}} \quad \alpha(\bar{x}) = \frac{E_x H R^2 \kappa(x)}{2\sqrt{D_{11}E_\theta H}} \quad \bar{\mathrm{m}} = \frac{\mathrm{M}}{2\pi R\sqrt{D_{11}E_\theta H}} \quad \bar{p} = \frac{pR^3}{3D_{22}}. \tag{39}$$

This leads to the definition of the following three non-dimensional parameters, referred to as the collapse parameter, tube length parameter and shear length parameter, respectively:

$$\chi = \sqrt{\frac{D_{11}E_\theta}{D_{22}E_x}} \quad \lambda = \sqrt[4]{\frac{9D_{22}L^4}{4E_x H R^6}} \quad \mu = \sqrt{\frac{G_{x\theta}L^2}{E_x R^2}}. \tag{40}$$

Then the coupled system for the solution of the Brazier problem becomes (primes represent $\mathrm{d}/\mathrm{d}\bar{x}$)

$$-\frac{\mu^2}{4\lambda^4}(\bar{w}''-\bar{u}')+(1+\bar{p})\bar{w} = \frac{\chi^2\alpha(\bar{x})^2}{3}, \quad \bar{u}''+\mu^2(\bar{w}'-\bar{u}) = 0,$$

$$\bar{\mathrm{m}} = \alpha(\bar{x})\left(1-\frac{3\bar{w}}{2}\right), \quad \bar{\alpha} = \int_0^1 \alpha(\bar{x})\,\mathrm{d}\bar{x}, \quad \begin{matrix}\bar{u}(0) = 0,\\ \text{-or-}\\ \bar{u}'(0) = 0,\end{matrix} \quad \bar{w}(0) = 0, \quad \bar{u}(1) = 0, \quad \bar{w}'(1) = 0. \tag{41}$$

Several limiting cases of the governing equations exist in terms of the nondimensional parameters $\chi$, $\lambda$ and $\mu$ of eqn (40). Firstly, as $\chi \to 0$, the forcing term in the second equation of eqn (41) disappears and the Brazier displacements $\bar{u}$ and $\bar{w}$ go to zero. For these small values of the collapse parameter $\chi$, the combination of a large axial stiffness $E_x$, which resists the curvature of the tube and a substantial circumferential bending stiffness $D_{22}$, which hampers the cross-sectional deformation, results in no Brazier effect being present. Conversely, large values of $\chi$ increase the influence of the Brazier phenomena for tubes under bending.

For the tube length parameter $\lambda$, the limiting cases can be written as:

$$\begin{aligned} \lambda \to 0 \quad &\Rightarrow \quad \bar{u}, \bar{w} = 0 \\ \lambda \to \infty \quad &\Rightarrow \quad \bar{u} = 0, \bar{w} = \text{constant}. \end{aligned} \tag{42}$$

The former case is for cylinders so short that the radial restraint totally nullifies the Brazier effect, while the latter case approaches an infinite length cylinder, which corresponds to Brazier's original solution in which the cross-sectional deformation is the same at all locations along the length. This solution has already been displayed in Fig. 2 and is represented as

$$\bar{u} = 0 \quad \bar{w} = \frac{\chi^2\bar{\alpha}^2}{3(1+\bar{p})} \quad \bar{\mathrm{m}} = \bar{\alpha}\left[1-\frac{\chi^2\bar{\alpha}^2}{2(1+\bar{p})}\right] \tag{43}$$

where $\bar{\alpha}$ is the normalized curvature of the tube axis and is now a constant.

Finally, the shear length parameter $\mu$ measures the extent of the shear boundary layer near the ends of the cylinder. For $\mu \to 0$, the shear stresses that arise from the transformation of the cross-section from an oval into a circle (at the restrained ends) are zero and the edge effects disappear, again leading to the infinite length solution of Brazier. Conversely, large

values of $\mu$ increase the boundary layer of the shear stresses and lead to the solution obtained by assuming that the shear strains are zero everywhere. Thus, ignoring the presence of the shear strain ($\mu \to \infty$) leads to the simplified system:

$$\frac{1}{4\lambda^4}\bar{w}'''' + (1+\bar{p})\bar{w} = \frac{\chi^2\alpha(\bar{x})^2}{3}, \quad \bar{m} = \alpha(\bar{x})\left(1-\frac{3\bar{w}}{2}\right), \quad \bar{\alpha} = \int_0^1 \alpha(\bar{x})\,d\bar{x},$$

$$\bar{w}'(0) = 0$$

$$\text{-or-} \quad , \quad \bar{w}(0) = 0, \quad \bar{w}'''(1) = 0 \quad \bar{w}'(1) = 0. \tag{44}$$

$$\bar{w}''(0) = 0$$

Note that for both systems eqns (41) and (44) the forcing term is dependent on $\alpha(\bar{x})$, not the constant $\bar{m}$, thereby making the equations nonlinear with respect to $\bar{w}(\bar{x})$. Numerical solutions and comparisons for variations of the non-dimensional parameters $\mu$ and $\lambda$, as well as the effect of the end conditions, will be discussed in the results.

## 3. LOCAL INSTABILITY

The solution of eqn (41) discloses that the moment vs end rotation curve is nonlinear and that it achieves a maximum limit moment when the deformed cross-section is no longer able to withstand the applied load. Many investigators have concluded that the failure of a tube, in the form of a kink on the compressive side of the cylinder, occurs when this limit moment is surpassed. In truth, this kink is a post-buckled state resulting from local buckling due to the compressive stresses at the top of the cylinder. In an earlier work by the present authors (1995), it was shown that this local buckling almost always occurs before the limit moment is reached. One possible exception is for multi-layered angle ply laminates with a large value of the collapse parameter $\chi$. In fact, $\chi$ is a measure of the ratio of the buckling moment (which is proportional to $\sqrt{D_{11}E_\theta}$) to the nonlinear limit moment (proportional to $\sqrt{D_{22}E_x}$), which is the reason it is termed the collapse parameter. Here we will restrict our study to single-layer laminates, composed of either isotropic or orthotropic materials, for which $\chi = 1$. For these structures, the buckling moment will always occur before the limit point is reached.

Buckling of circular cylinders under bending was most qualitatively defined by Seide and Weingarten (1961). They determined that the maximum critical bending stress is roughly equal to the critical buckling stress under axial compression. Local buckling occurs when the maximum compressive stress (at $\theta = 0$) attains this value. For orthotropic materials, this critical stress is

$$\sigma_{cr} = \frac{-2\sqrt{D_{11}E_\theta H}}{\rho H} \tag{45}$$

where $\rho$ is the local radius of the cylinder at $\theta = 0$. Due to the Brazier effect, the cross-section of the cylinder deforms into an oval and the radius of curvature at the critical location increases (see Fig. 1), thus lowering the critical buckling stress. Therefore, we can get a good estimate of the collapse moment by determining when the axial stress on the compressive side of the cylinder reaches this critical value. Of course, a more reliable determination of the collapse load would be to perform a stability analysis from the nonlinear prebuckled state. However, we will employ this Seide–Weingarten approximation since it is computationally simple and reveals the important points of local buckling in a straightforward manner.

Only two characteristics of the loaded cylinder need be known to determine stability under this criterion, the axial stress resultant and the circumferential curvature. Both quantities have already been defined in terms of the Brazier displacements $u_2$ and $w_2$ through eqns (8) and (14). Here we rewrite the relations in non-dimensional form as

$$\bar{\kappa}_\theta = R\kappa_\theta = -3\bar{w}(\bar{x})\cos 2\theta$$

$$n_x = \frac{-N_x R}{2\sqrt{D_{11}E_\theta H}} = -\frac{3}{4\chi\lambda^2}\bar{u}'(\bar{x})\cos 2\theta + \alpha(\bar{x})\left[\left(1-\frac{3\bar{w}(\bar{x})}{4}\right)\cos\theta - \frac{\bar{w}(\bar{x})}{4}\cos 3\theta\right]. \quad (46)$$

Then the stipulation that the maximum compressive stress (at $\theta = 0$) must remain below the critical buckling stress to remain stable

$$\frac{N_x(\theta=0)}{H} < \frac{-2\sqrt{D_{11}E_\theta H}}{H}\left[\frac{1}{R} + \kappa_\theta(\theta=0)\right] \quad (47)$$

generates the stability criterion for orthotropic tubes of arbitrary length

$$\alpha(\bar{x})[1-\bar{w}(\bar{x})] - \frac{3}{4\chi\lambda^2}\bar{u}'(\bar{x}) < 1-3\bar{w}(\bar{x}). \quad (48)$$

This criterion must be investigated at all points along the length of the cylinder. Usually the solution for the displacements is computed numerically for a given loading parameter $\bar{\alpha}$ and the axial stress resultant and buckling envelope are calculated at finite points in the domain. Buckling occurs when the inequality of eqn (48) is first violated and the kink should form at that axial location.

## 4. NUMERICAL RESULTS

The coupled nonlinear systems eqns (41) and (44) are solved numerically using finite difference techniques and Newton's method. Though analytical solutions could be obtained for certain cases of the non-dimensional parameters, the numerical technique is suitably efficient to fully explore the effects of the parameters on the solution, as well as being computationally inexpensive enough to use in full scale optimization studies. For this investigation, the cylinder was assumed to be unpressurized ($\bar{p} = 0$) with a collapse parameter $\chi$ equal to one, thereby rendering the solution dependent solely on the tube length parameter $\lambda$ and the shear length parameter $\mu$. Stability is assessed through eqn (48) and the moment vs end rotation curves terminate when the Seide–Weingarten criterion is violated.

### 4.1. *General solution for $\lambda$ and $\mu$*

The applied bending moment as a function of end rotation is shown in Fig. 5 for various values of $\mu$ when $\lambda = 1$. Note that the smaller values of $\mu$ increase the nonlinear effect and lead to lower buckling loads. This is due to the fact that small values of the shear length parameter generate larger shear deformation, thereby allowing additional degrees of freedom and less stiff structures. For $\mu > 5$ in Fig. 5, the solution approaches the case of no shear strain ($\mu \to \infty$), which corresponds to the system of eqn (44).

Keeping $\mu$ constant and stipulating various values of $\lambda$ leads to the load–displacement curves of Fig. 6. Small values of the tube length parameter correspond to short and thin cylinders which do not undergo ovalization, thus remaining linear and buckling at the classical value. As $\lambda$ increases, the effect of the Brazier nonlinearity does too, until it approaches the infinite length solution given by eqn (43). For this case, the stability criterion of eqn (48) yields for the buckling loads:

$$\bar{\alpha}_\infty = 0.66012 \quad \bar{m}_\infty = 0.51629 \quad \bar{w}_\infty = 0.14525. \quad (49)$$

Collapse loads due to local buckling are shown as a function of $\lambda$ and $\mu$ as a surface plot in Fig. 7a. The contour lines correspond to constant values of the critical buckling curvature $\bar{\alpha}_{cr}$. One can see that as the shear length parameter $\mu$ increases, the contour lines become parallel, indicating that changes in the value of $\mu$ do not significantly affect the

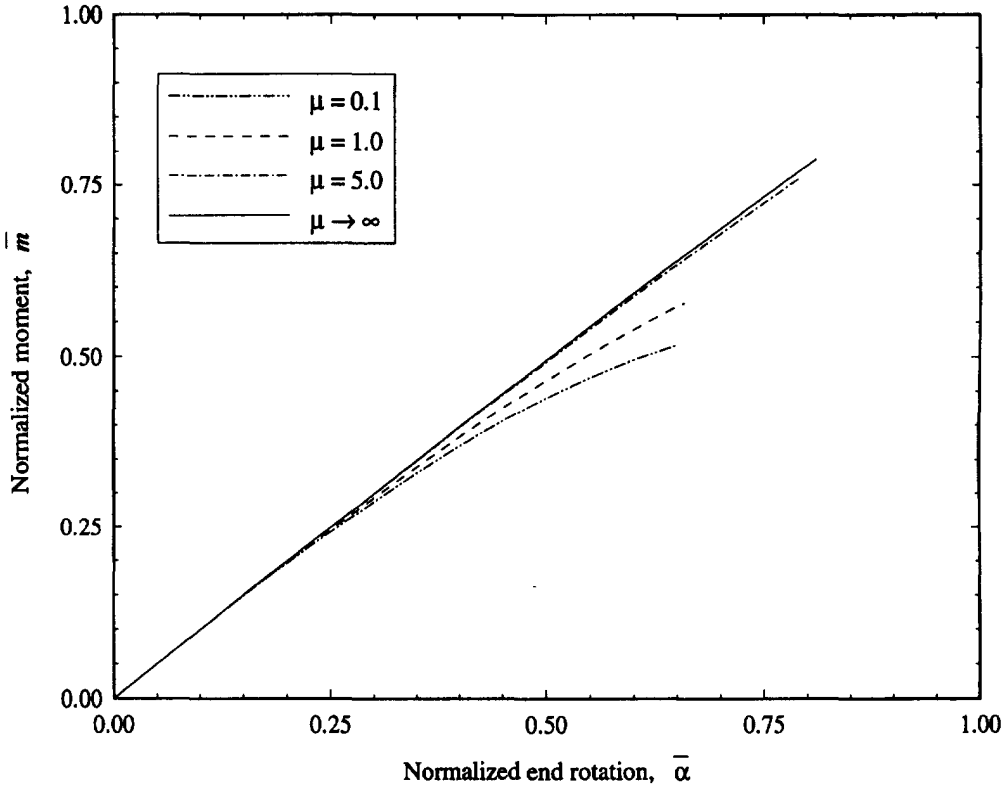


Fig. 5. Moment vs end rotation for $\lambda = 1$, fixed ends.

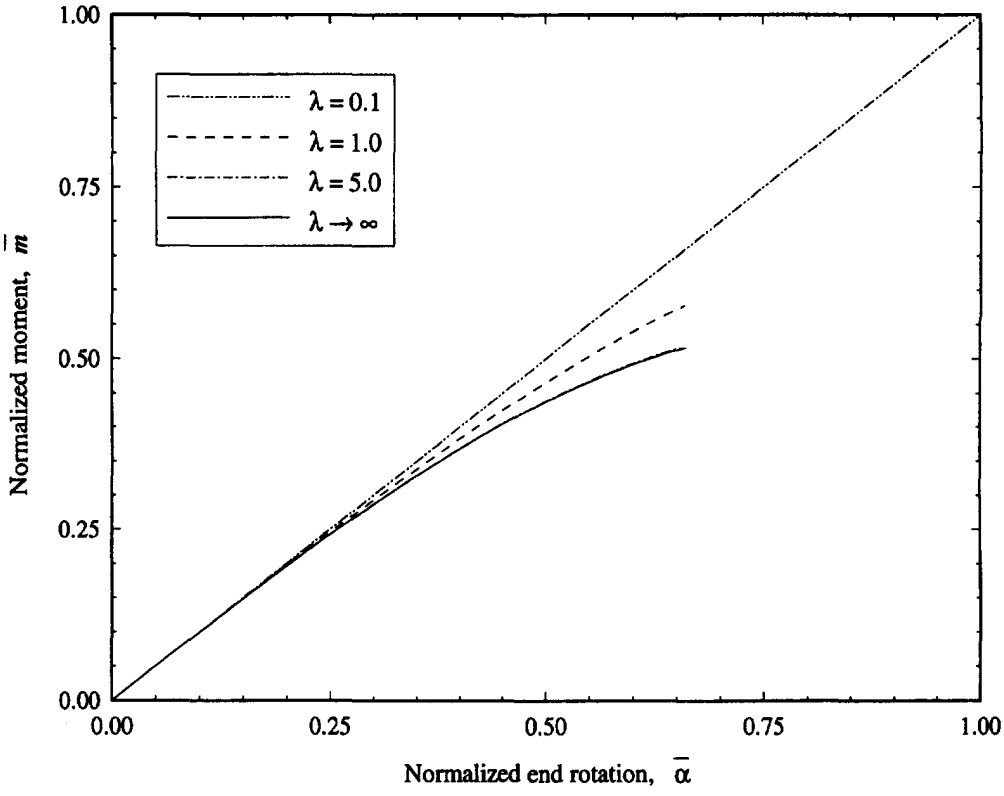


Fig. 6. Moment vs end rotation for $\mu = 1$, fixed ends.

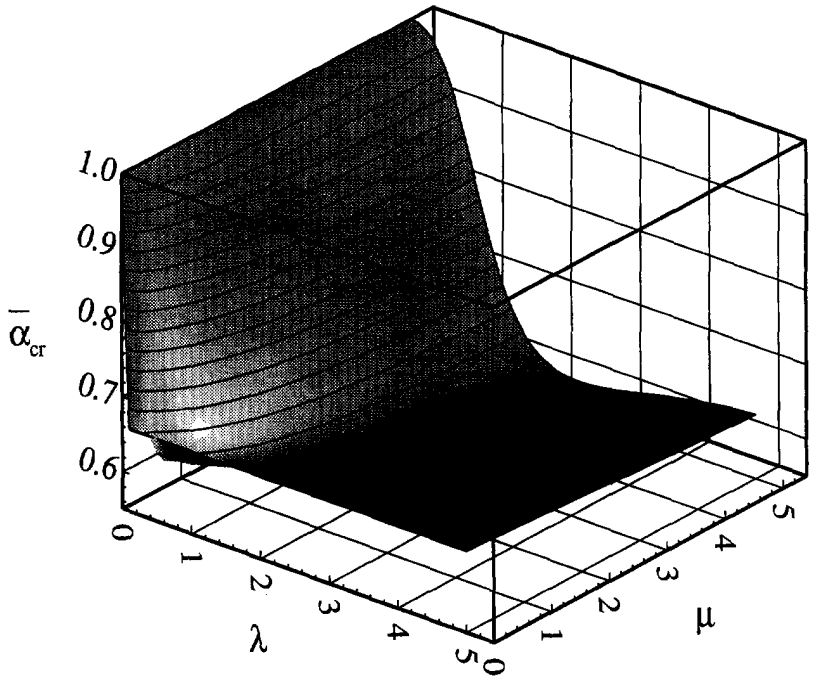


(a)

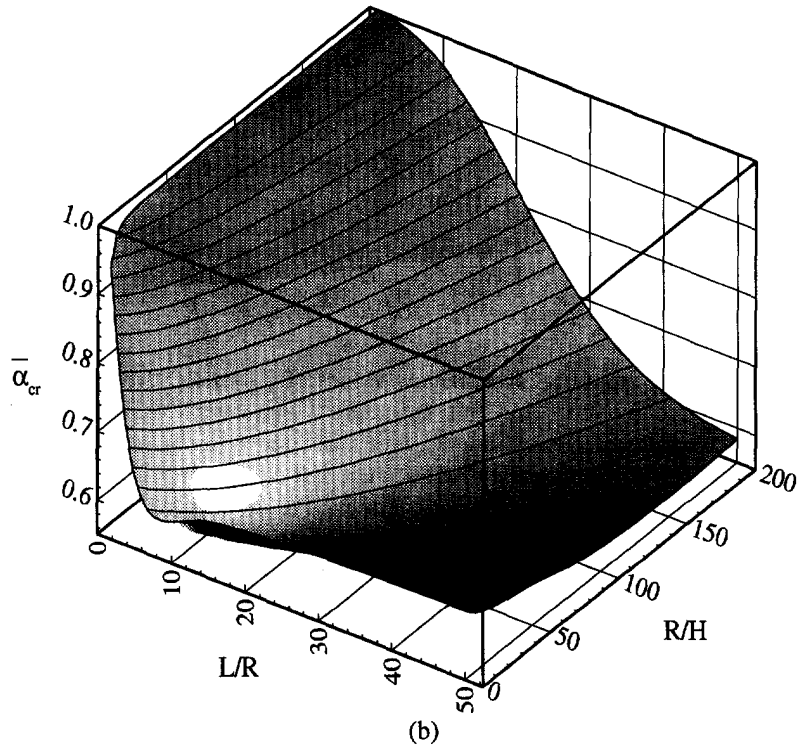


(b)

Fig. 7. Critical curvature for fixed end cylinders.

solution if $\mu$ is greater than around five. For these regions, the collapse behavior is governed by the tube length parameter $\lambda$. Also note that many areas of the surface have critical curvatures which are below the infinite length value as given by eqn (49). This is due to the edge effects at the boundaries propagating throughout the structure and significantly altering the values of the axial stress resultant and circumferential curvature.

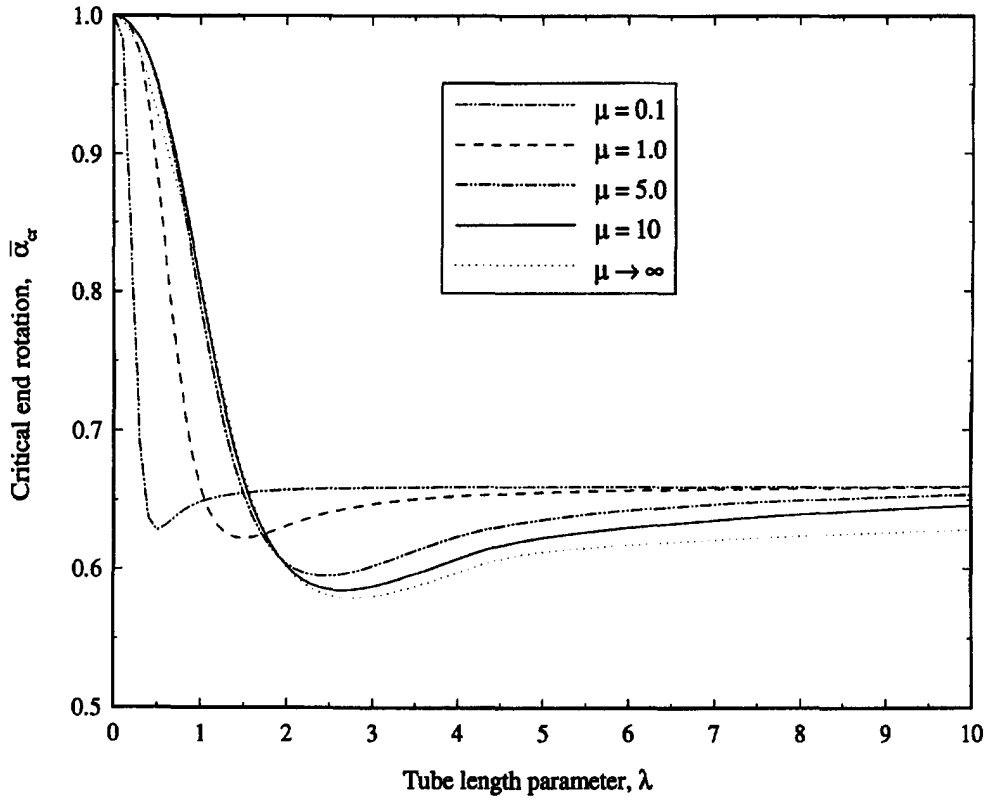


Fig. 8. Critical curvature vs tube length parameter for general material, fixed ends.

To give greater physical feel to the parameters $\lambda$ and $\mu$, we express them both in terms of a "material" and "geometric" portion:

$$\lambda = \sqrt[4]{\frac{9D_{22}}{4E_xH^3}} \cdot \frac{L}{R}\sqrt{\frac{H}{R}} \quad \mu = \sqrt{\frac{G_{x\theta}}{E_x}} \cdot \frac{L}{R}. \tag{50}$$

Therefore, for a given material system, low values of $\lambda$ (which produce very little Brazier effect) are generated by short and thin cylinders which buckle according to the classical solution. Longer and thicker cylinders, which are more easily constructed as "tubes", undergo drastic Brazier nonlinearity before buckling occurs. Additionally, the importance of the shear strain is only seen for shorter cylinders, i.e. small values of $\mu$. Similar arguments could be made for the material portion of eqn (50), though the range of parameter values for typical material systems does not vary as greatly as those of the geometric part. To illustrate the point further, a surface plot for the critical curvatures of an isotropic cylinder as a function of length-to-radius ratio $L/R$ and radius-to-thickness ratio $R/H$ is displayed in Fig. 7b. As expected, short and thin cylinders undergo little Brazier nonlinearity, while the longer, thicker, tube-like cylinders behave closer to the infinite length case. Figure 7 also reveals why we prefer to employ the non-dimensional parameters $\lambda$ and $\mu$, as they approach a definite solution as they tend toward infinity.

### 4.2. *Influence of shear length parameter*

We have seen in Fig. 7a that the nonlinear solution does not significantly change for larger values of $\mu$. This must be investigated in greater detail, for if we can ignore the presence of shear strain (when $\mu \to \infty$) we can reduce the system of eqn (41) to the single ordinary differential equation of eqn (44), thereby increasing the efficiency of the solution technique. To this end, the critical buckling curvature is shown as a function of the tube length parameter $\lambda$ for various values of the shear length parameter $\mu$ in Fig. 8. The

asymptote that the curves all approach as $\lambda \to \infty$ is the infinite tube solution of eqn (49). Small values of $\mu$ arrive at this asymptote quite quickly, and the effect of ignoring the shear strain for the Brazier problem ($\mu \to \infty$) can lead to serious errors in the calculation of the buckling load. However, Fig. 8 may be misleading in regard to the range of values that $\mu$ can achieve. For instance, specification of the material system for the cylinder under bending puts a lower bound on the value of $\mu$ with respect to $\lambda$, since from eqn (50)

$$\mu = \sqrt[4]{\frac{4G_{x\theta}^2 H^3}{9E_x D_{22}}} \cdot \sqrt{\frac{R}{H}} \cdot \lambda. \tag{51}$$

The ratio of $R/H$ must be greater than one half, else the structure is not a cylinder. In fact, the ratio should be roughly greater than 20, else the thin cylinder assumptions may not hold. Therefore, values of $\mu = 1$ for large values of $\lambda$ may not even be feasible. For instance, Fig. 8 is reproduced for an isotropic cylinder for various values of radius-to-thickness ratios in Fig. 9a. One can see that all of the different thickness cylinders produce remarkably similar solutions, and that they all approach the case which ignores the presence of the shear strain. The largest deviation from this case occurs for shorter, thicker cylinders, as expected. Similar results apply even to highly orthotropic materials, such as the graphite–epoxy AS3501 used by Corona and Rodrigues (1995) for the study of infinite length tubes under bending. For this material, $E_1/G_{12}$ is around 20 and $E_1/E_2$ approximately 15, yet Fig. 9b reveals that this material also approaches the case of no shear for thinner shells. Therefore, one can conclude that the shear warping of Fig. 4 is not significant for most thin shells under pure bending and that the simpler system of eqn (44) can be used except for small values of $\lambda$ and $\mu$.

4.3. *Influence of boundary conditions*

The results presented so far have all been generated with the "fixed end" boundary condition. We consider this case more realistic, since most testing apparatus and structural applications involve a rigid plate or sturdy ring stiffener at the end of the cylinder. However, the "free end" boundary condition can occur in other tube bending applications, or more commonly, an elastic restraint which lies between the limiting cases of fixed and free is present. Therefore, it is informative to investigate the effect of the boundary conditions on the buckling characteristics and load–displacement behavior.

The surface image of Fig. 7 for a fixed end cylinder is reproduced in Fig. 10 as a contour plot, along with the corresponding level lines for a tube with free ends (dashed lines). Regions where the contours coincide are the values of $\lambda$ and $\mu$ for which the boundary effects have no effect. According to Fig. 10, this is true for small values of $\mu$, which approaches the infinite length case as it goes to zero, as stated earlier. Though not evident on the scale of Fig. 10, very small and very large values of $\lambda$ also are independent of boundary conditions. The small values of $\lambda$ experience no Brazier deformation, while the large values approach the infinite case for which the boundary conditions have no effect. For all intermediate values of both parameters, however, the response does vary significantly according to the end condition. In general, the free end allows for greater movement, thus producing more nonlinear ovalization and lower buckling loads.

As an illustration of this, load–displacement curves and buckling load comparisons are performed for both end conditions for an isotropic cylinder with $R/H = 100$. First, moment and radial displacement vs end rotation for $\lambda = 2$ are shown in Fig. 11. As expected, the fixed end generates a stiffer structure due to the extra restraint applied to the displacements. Shown in Fig. 12 is the critical end rotation and bending moment as a function of $\lambda$. Note that the moments approach the asymptotic value of the infinite length case much faster than the end rotations, due to the small slope of the load–displacement relation near collapse.

4.4. *Comparison to published results*

Few references exist concerning finite length tubes that are long enough for the Brazier effect to be significant. Most cylinders in structural applications are short or have ring

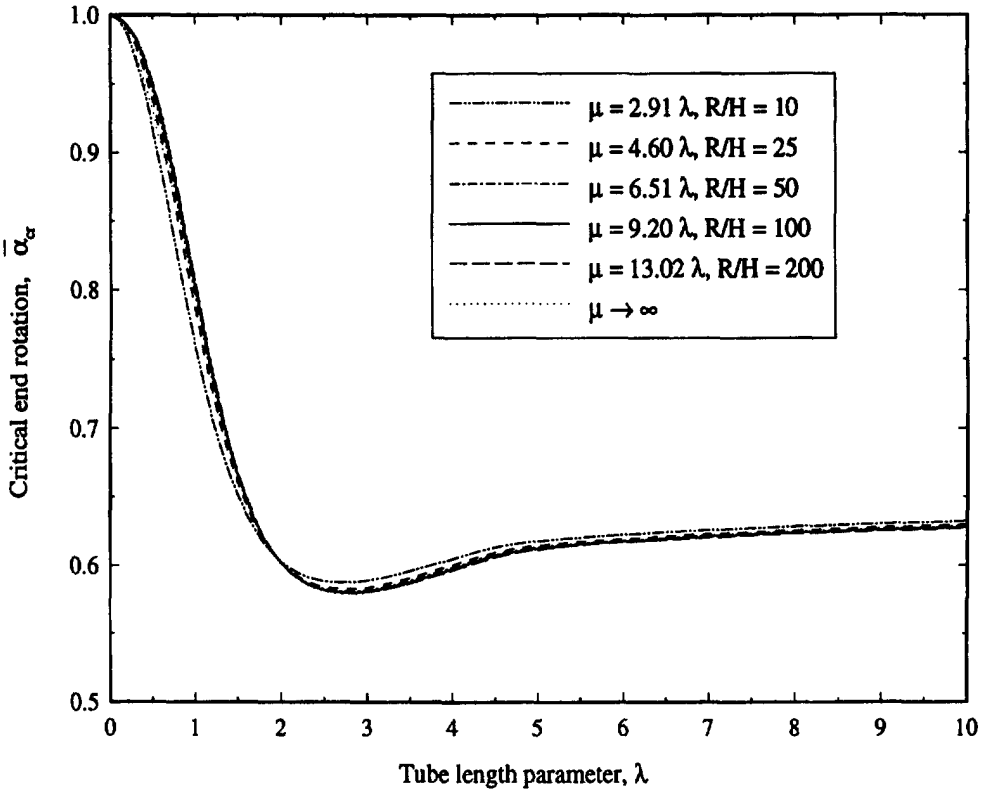


(a) Isotropic, ν = 0.3

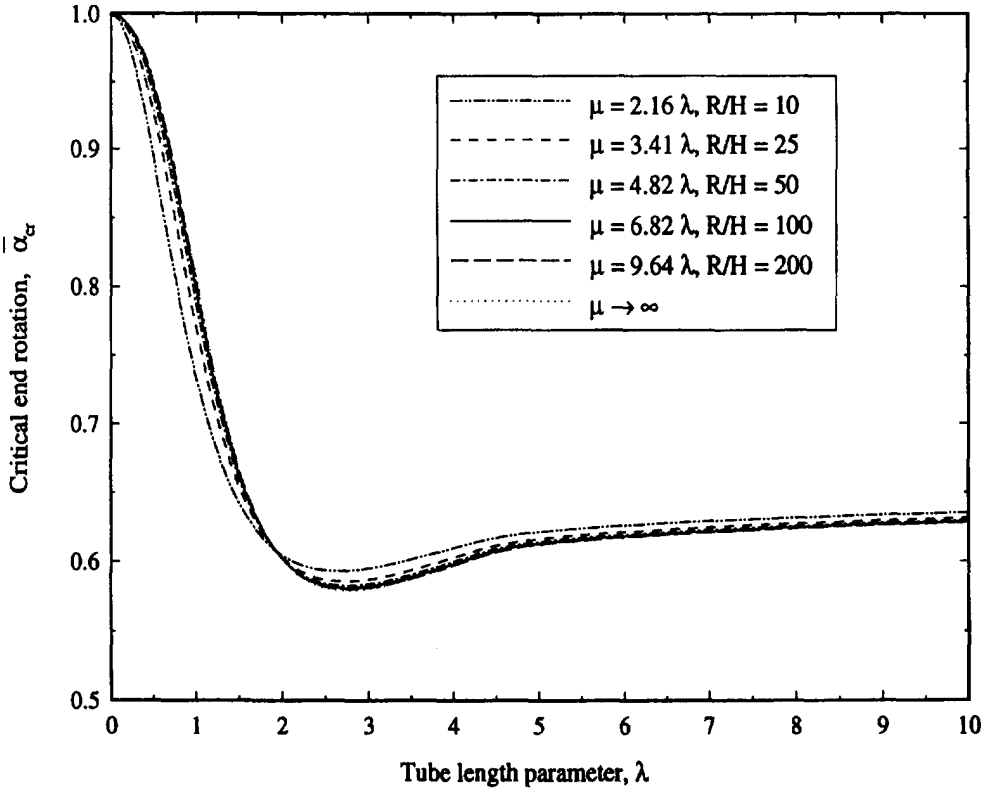


(b) Orthotropic, AS3501

Fig. 9. Critical curvature vs tube length parameter for specific materials, fixed ends.

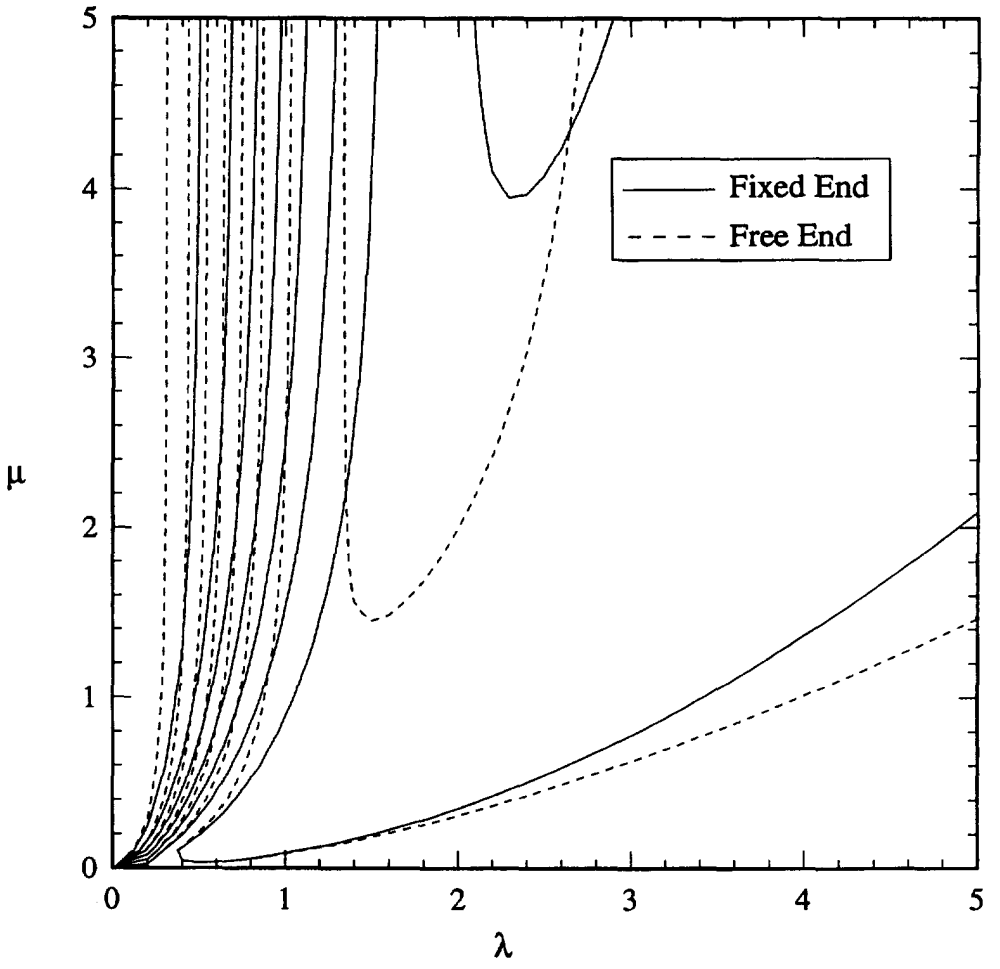


Fig. 10. Comparison of critical curvature for fixed and free end conditions.

stiffeners that inhibit the nonlinear ovalization. However, Stephens *et al.* (1975) performed a nonlinear finite element analysis on various length isotropic cylinders under bending and pressure to measure the amount of ovalization and nonlinearity due to the Brazier effect. Their results are presented in terms of the amount of ovalization vs the applied bending moment and are reproduced here in Fig. 13 and compared to the present analysis (the free end condition is used for both analyses). The curves from Stephens *et al.* (1975) end when a critical buckling moment is determined, which is calculated from the nonlinear equilibrium state by determining when the amplitude of an axial wrinkle (introduced as an imperfection) increases dramatically for small increases in the load. However, the choices for the shape of this buckled state are limited, thereby leading to overestimations of the buckling values and an incorrect asymptote for longer tubes (the collapse envelope for infinite length tubes actually approaches the value of the limit load instead of the buckling point of eqn (49)). Except for this discrepancy for the longer tubes, the comparison of Fig. 13 reveals that our simpler solution does agree along basic trends with the rigorous nonlinear solution. Further comparisons with more accurate finite element solutions must also be performed in the future.

A more recent investigation of the Brazier effect for finite length tubes was performed by Libai and Bert (1994), who employed semi-membrane theory and the approximations of Brazier to produce systems analogous to eqns (41) and (44). Approximate closed form solutions using a simple Rayleigh analysis were generated for orthotropic tubes under the assumption that the shear strain is zero ($\mu \to \infty$). Critical loads due to local buckling were estimated along the same lines as those presented here, and their solution for the buckling moments of isotropic tubes are compared to the present work in Fig. 14. For small values

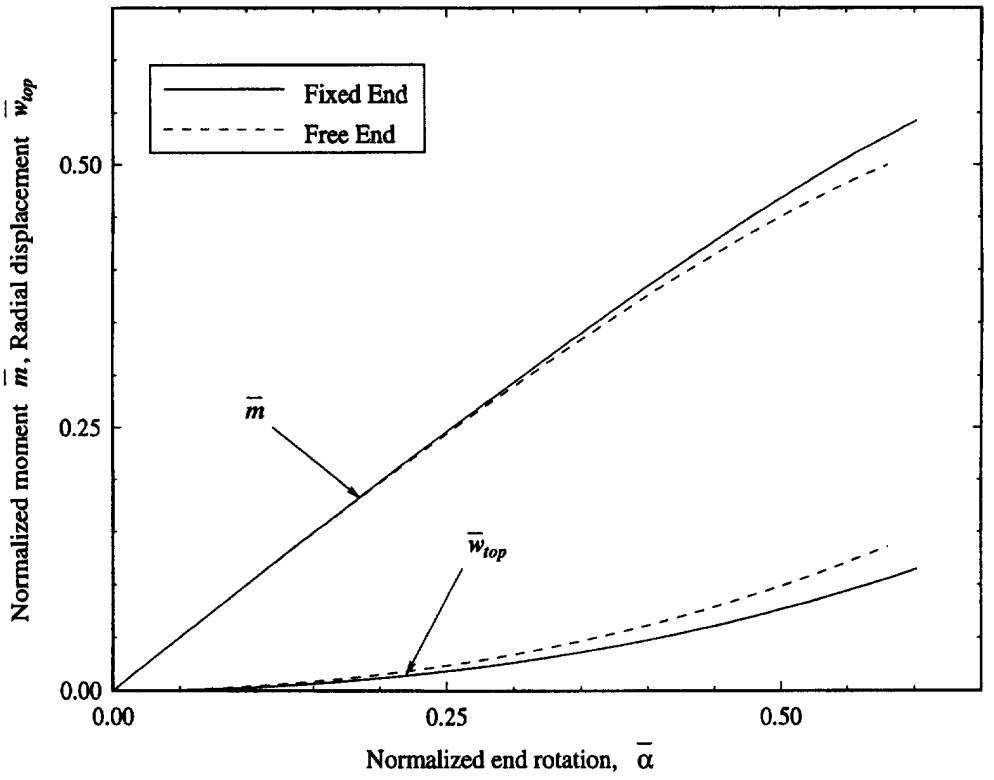


Fig. 11. Comparison of load–displacement curves for fixed and free end conditions for isotropic cylinder.

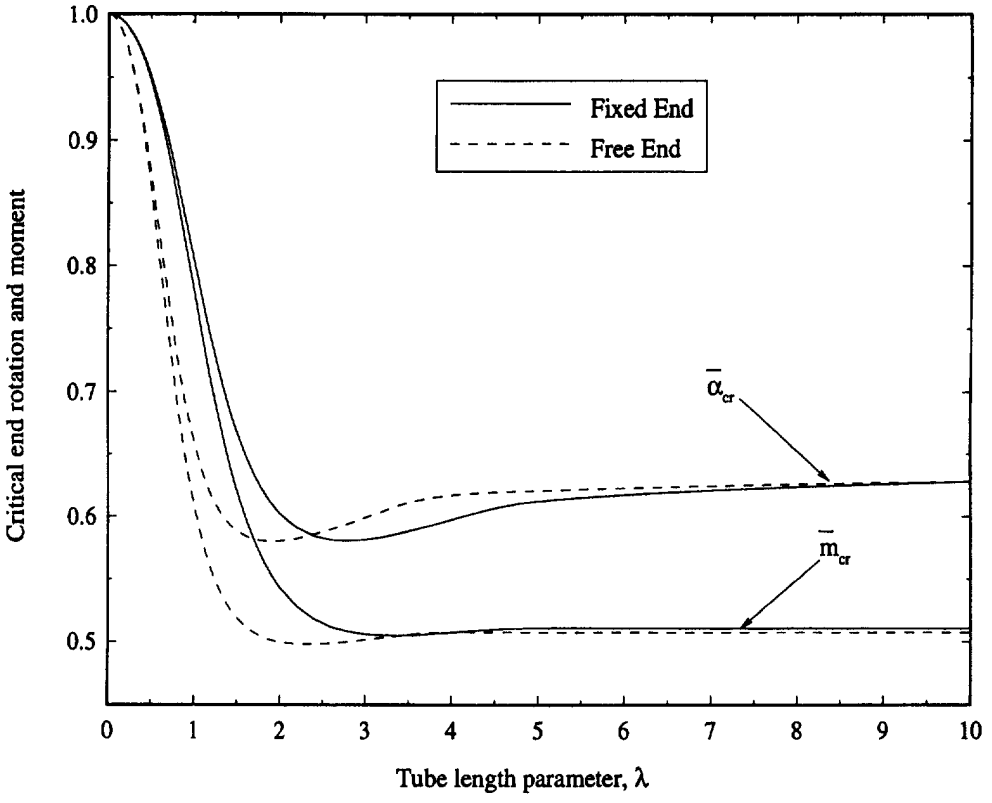


Fig. 12. Comparison of critical curvature for fixed and free end conditions for isotropic cylinder.

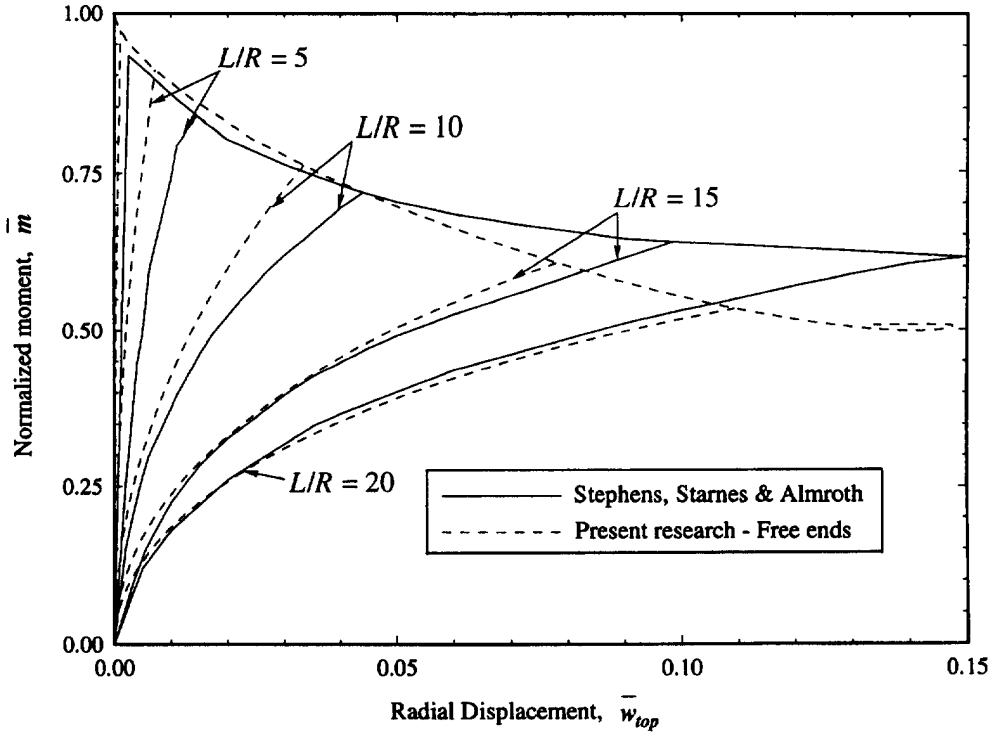


Fig. 13. Comparison to Stephens *et al.* for moment vs radial displacement.

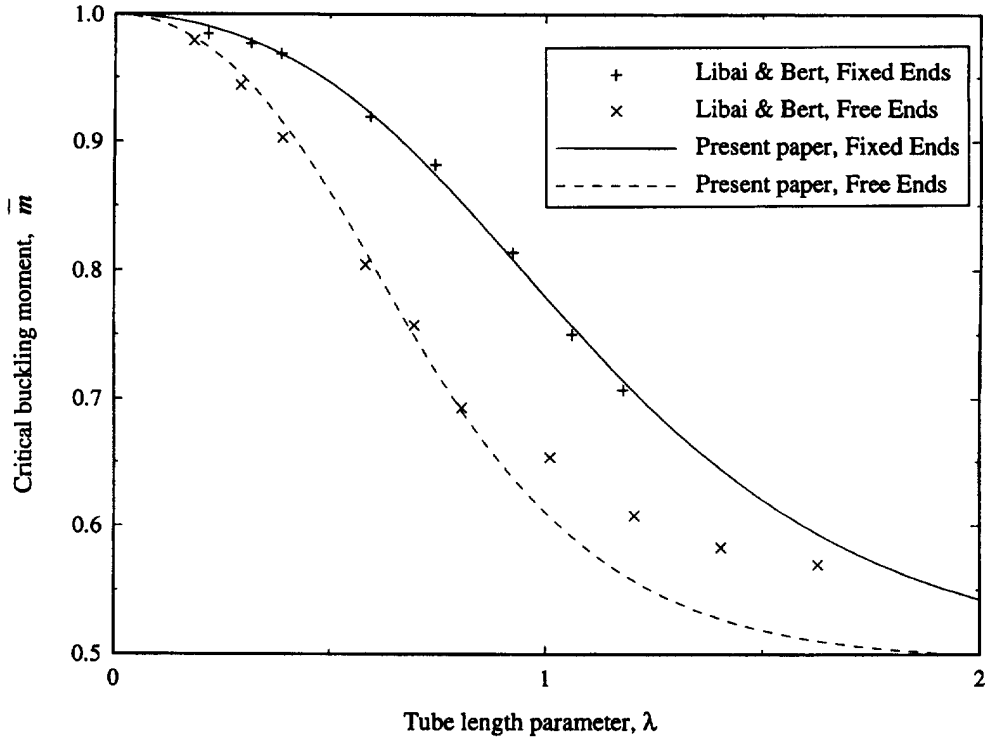


Fig. 14. Comparison to Libai and Bert for critical moments for isotropic material.

of $\lambda$, a slight discrepancy exists due to the inclusion of shear strain in our analysis. This difference seems negligible in Fig. 14, however it should be realized that the critical load is presented in terms of the moment as opposed to the end rotation, which tends to minimize the differences due to the small slope of the load–displacement curve near the critical point. The larger discrepancy occurs in Fig. 14 for longer cylinders with the free end boundary

condition, where Libai and Bert have used a Rayleigh technique to solve the nonlinear differential equations. This larger error is due to the approximate solution underestimating the nonlinearity and producing a higher buckling moment.

## 5. CONCLUSIONS

The equations governing the nonlinear bending response of finite length composite tubes that exhibit Brazier's cross-sectional deformation are derived using classical shell theory along with the assumptions of semi-membrane constitutive theory and the linearization of Brazier. A simple criterion for determining local instability is also employed, and this buckling estimation along with the system of ordinary differential equations is solved using numerical methods.

The results presented have shown that the assumption of zero shear strain for a tube under pure bending is only violated for small values of the parameter $\mu$, which correspond to short cylinders that do not have a high shear stiffness. The dominant parameter influencing the load–displacement response and collapse due to local buckling is the tube length parameter $\lambda$. Furthermore, it was proven that the membrane boundary conditions of either a fixed or free end is important for almost all values of the cylinder parameters, with the fixed end condition generally producing stiffer structures and higher buckling loads.

*Acknowledgements*—The work reported herein was supported in part by a grant from NASA Langley Research Center, NAG-1-643. The support for the work of the first two authors is gratefully acknowledged.

## REFERENCES

Aksel'rad, E. L. (1965) Pinpointing the upper critical bending load of a pipe by calculating geometric nonlinearity. *Izv. Akad. Nauk SSR Mekh.* **4,** 133–139.

Aksel'rad, E. L. and Emmerling, F. A. (1984) Collapse load of elastic tubes under bending. *Isr. Journal of Technology* **22,** 89–94.

Bannister, K. A. (1984) Direct energy minimization to whipping analysis of pressure hulls. *Shock Vibrations Bulletin* **54,** 67–85.

Brazier, L. G. (1926) The flexure of thin cylindrical shells and other 'thin' sections. *Late of the Royal Aircraft Establishment.* Reports and Memoranda No. 1081 (M.49), pp. 1–30.

Calladine, C. R. (1983) *Theory of Shell Structures.* Cambridge University Press, Cambridge.

Corona, E. and Rodrigues, A. (1995) Bending of long cross-ply composite circular cylinders. *Composite Engineering* **5,** 163–182.

Fabian, O. (1977) Collapse of cylindrical, elastic tubes under combined bending, pressure and axial loads. *International Journal of Solids and Structures* **13,** 1257–1270.

Jones, R. M. (1975) *Mechanics of Composite Materials.* Hemisphere Publishing Company, Washington, DC.

Libai, A. and Bert, C. W. (1994) A mixed variational principle and its application to the nonlinear bending problem of orthotropic tubes—II. Application to nonlinear bending of circular cylindrical tubes. *International Journal of Solids and Structures* **31,** 1019–1033.

Novoshilov, V. V. (1959) *The Theory of Thin Shells* (Translated by P. G. Lowe). P. Noordhoff Ltd, The Netherlands.

Reissner, E. (1959) On finite bending of pressurized tubes. *Journal of Applied Mechanics* **26,** 386–392.

Sanders, Jr, J. L. (1963) Nonlinear theories for thin shells. *Quarterly of Applied Mathematics* **21,** 21–36.

Seide, P. and Weingarten, V. I. (1961) On the buckling of circular cylindrical shells under pure bending. *Journal of Applied Mechanics* **28,** 112–116.

Stephens, W., Starnes, Jr, J. H. and Almroth, B. O. (1975) Collapse of long cylindrical shells under combined bending and pressure loads. *AIAA Journal* **13,** 20–25.

Tatting, B. F., Gürdal, Z. and Vasiliev, V. V. (1995) Nonlinear shell theory solution for the bending response of orthotropic finite length cylinders including the Brazier effect. *Proc. 36th Structures, Structural Dynamics and Materials Conf.* New Orleans, LA, pp. 966–976.

Tatting, B. F., Gürdal, Z. and Vasiliev, V. V. (1996) Nonlinear response of long orthotropic tubes under bending including the Brazier effect. *AIAA Journal* **34,** 1934–1940.

Vasiliev, V. V. (1993) *Mechanics of Composite Structures.* Taylor and Francis, Washington, DC.

Wood, J. D. (1958) The flexure of a uniformly pressurized circular, cylindrical shell. *Journal of Applied Mechanics* **80,** 453–458.